INTERFACE SCIENCE AND TECHNOLOGY – VOLUME 11

Surface Complexation Modelling

Edited by

Johannes Lützenkirchen

Institut für Nukleare Entsorgung
Forschungszentrum Karlsruhe
Karlsruhe, Germany

ELSEVIER

Amsterdam • Boston • Heidelberg • London • New York • Oxford
Paris • San Diego • San Francisco • Singapore • Sydney • Tokyo
Academic Press is an imprint of Elsevier

Surface Complexation Modelling
J. Lützenkirchen (editor)
Published by Elsevier Ltd.

Chapter 18

Prediction of anion adsorption and transport in soil systems using the constant capacitance model

S. Goldberg and D.L. Suarez

USDA-ARS, George E. Brown, Jr. Salinity Laboratory, 450 W. Big Springs Road, Riverside, California, 92507, USA

1. INTRODUCTION

Boron, molybdenum, and arsenic are trace elements that can become elevated in soils and waters.

- Boron is an essential micronutrient element required for plant growth that is toxic at high concentration. Crop yield losses can occur both under conditions of B deficiency and B toxicity.
- Molybdenum is also an essential micronutrient element for plants that is potentially toxic, especially to grazing ruminant animals. Cattle grazing on legumes on alkaline soils can be adversely affected by elevated Mo content.
- Arsenic is toxic to both animals and plants. Arsenic concentrations in waters and soils can become elevated as a result of application of arsenical pesticides, disposal of fly ash, mineral dissolution, mine drainage, and geothermal discharge. In oxidizing aerobic environments, the stable form of inorganic As is arsenate, As(V).

Adsorption of trace elements on soil surfaces is an important process in managing trace element toxicity or deficiency as well as trace element concentrations in discharge waters. Increasing demands for high quality water in arid and semi arid regions are coupled with environmental concerns and constraints of the discharge of agricultural drainage waters. A major part of these environmental concerns in the southwestern United States and elsewhere is related to discharge of the oxyanions Se, As and B. Agriculture must utilize low quality waters for irrigation in addition to using drainage waters. The high concentrations of trace elements may also adversely affect plant growth.

Availability of trace elements to plants is affected by a variety of factors including soil pH, soil texture, soil moisture, temperature, oxide content, carbonate content, organic matter content, and clay mineralogy. The adsorbing surfaces in soils are oxides, clay minerals, calcite, and organic matter.

Careful quantification of soil solution trace element concentrations and characterization of trace element adsorption reactions on soil surfaces is needed. There are currently restrictions on discharge of oxyanions from drainage waters into many surface streams and rivers in the southwestern US. There is a clear need to predict oxyanion concentrations in drainage waters including how changes in soil management will impact the subsurface adsorption and transport. In addition, water quality criteria for irrigation currently neglect the impact of adsorption to alter the soil solution composition, thus many drainage waters are considered unsuitable for reuse. As will be demonstrated, management options can utilize the non-steady state dynamics of adsorption and desorption.

2. CONSTANT CAPACITANCE MODEL

The constant capacitance model is a surface complexation model that was developed by the research groups of Schindler and Stumm for the oxide-solution interface [1, 2]. As is characteristic of surface complexation models, this model explicitly defines surface species, chemical reactions, equilibrium constant expressions, and electrostatic potential effects. The surface functional group is defined as SOH, an average reactive surface hydroxyl ion bound to a metal, S, in the oxide mineral. Adsorbing ions are assumed to form strong inner-sphere complexes, located in a surface plane along with the protons and hydroxyl ions. Inner-sphere complexes contain no water between the adsorbing ion and the surface functional group. The present study will treat the extension of the constant capacitance model to describe and predict adsorption of the trace element anions: borate, molybdate, and arsenate on soil surfaces.

2.1. Model assumptions

The constant capacitance model contains the following assumptions: 1) all surface complexes are inner-sphere; 2) anion adsorption occurs via a ligand exchange mechanism with reactive surface hydroxyl groups; 3) no surface complexes are formed with ions from the background electrolyte; 4) the relationship between surface charge, σ ($mol_c\ L^{-1}$), and surface potential, ψ (V), is linear and given by:

$$\sigma = \frac{CSa}{F}\psi \qquad (1)$$

where C ($F\ m^{-2}$) is the capacitance, S ($m^2\ g^{-1}$) is the surface area, a ($g\ L^{-1}$) is the particle concentration, and F ($C\ mol_c^{-1}$) is the Faraday constant. Placement of ions in the constant capacitance model is indicated in Fig. 1.

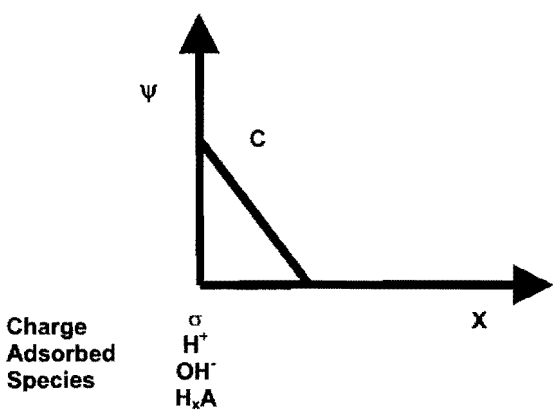

Fig.1. Placement of ions, charge, surface charge, and surface potential for the constant capacitance model where A represents the oxyanion, and x is the number of dissociations undergone by the acid.

2.2. Surface chemical reactions

In the constant capacitance model the protonation and dissociation reactions of the surface functional group are:

$$SOH + H^+ \rightleftharpoons SOH_2^+ \tag{2}$$

$$SOH \rightleftharpoons SO^- + H^+ \tag{3}$$

For soil systems the SOH group is generic and represents reactive aluminol and silanol groups on the edges of clay mineral particles, as well as surface hydroxyls on oxides. The surface complexation reactions for the adsorption of borate, molybdate, and arsenate are:

$$SOH + H_3BO_3 \rightleftharpoons SH_3BO_4^- + H^+ \tag{4}$$

$$SOH + H_2MoO_4 \rightleftharpoons SHMoO_4 + H_2O \tag{5}$$

$$SOH + H_3AsO_4 \rightleftharpoons SH_2AsO_4 + H_2O \tag{6}$$

$$SOH + H_3AsO_4 \rightleftharpoons SHAsO_4^- + H^+ + H_2O \tag{7}$$

$$SOH + H_3AsO_4 \rightleftharpoons SAsO_4^{2-} + 2H^+ + H_2O \tag{8}$$

2.3. Equilibrium constants

The intrinsic equilibrium constant expressions for the above reactions are:

$$K_+(\text{int}) = \frac{[SOH_2^+]}{[SOH][H^+]}\exp(F\psi / RT) \tag{9}$$

$$K_-(\text{int}) = \frac{[SO^-][H^+]}{[SOH]}\exp(-F\psi / RT) \tag{10}$$

$$K_{B-}(\text{int}) = \frac{[SH_3BO_4^-][H^+]}{[SOH][H_3BO_3]}\exp(-F\psi / RT) \tag{11}$$

$$K_{Mo}(\text{int}) = \frac{[SHMoO_4]}{[SOH][H_2MoO_4]} \tag{12}$$

$$K_{As}^1(\text{int}) = \frac{[SH_2AsO_4]}{[SOH][H_3AsO_4]} \tag{13}$$

$$K_{As}^2(\text{int}) = \frac{[SHAsO_4^-][H^+]}{[SOH][H_3AsO_4]}\exp(-F\psi / RT) \tag{14}$$

$$K^3_{As}(\text{int}) = \frac{[SAsO_4^{2-}][H^+]^2}{[SOH][H_3AsO_4]} \exp(-2F\psi / RT) \quad (15)$$

2.4. Activity coefficients

In the constant capacitance model the standard state for surface complexes is a chargeless environment [3]. The intrinsic equilibrium constants are directly proportional to the thermodynamic equilibrium constants. Charged surface complexes create an average electric potential field at the particle surface. These coulombic forces provide the dominant contribution to the solid-phase activity coefficients, while the contribution from other forces is considered equal for all surface complexes. In this manner, the exponential terms can be considered as solid phase activity coefficients [3].

With the addition of a mass balance equation and a charge balance equation, the system can be solved using a mathematical approach. The computer program FITEQL [4] is an iterative nonlinear least squares optimization program that can be used to fit equilibrium constants to experimental data and contains the constant capacitance model of adsorption. The program can also be used to predict chemical speciation using previously determined equilibrium constant values. Stoichiometry of the equilibrium problem for the application of the constant capacitance model to borate, molybdate, and arsenate adsorption is provided in Table 1.

Table 1
Stoichiometry of the equilibrium problem for the constant capacitance model

	Components			
Species	SOH	$e^{F\psi/RT}$	H_xA	H^+
H^+	0	0	0	1
OH^-	0	0	0	-1
SOH_2^+	1	1	0	1
SOH	1	0	0	0
SO^-	1	-1	0	-1
H_3BO_3	0	0	1	0
$B(OH)_4^-$	0	0	1	-1
H_2MoO_4	0	0	1	0
$HMoO_4^-$	0	0	1	-1
MoO_4^{2-}	0	0	1	-2
H_3AsO_4	0	0	1	0
$H_2AsO_4^-$	0	0	1	-1
$HAsO_4^{2-}$	0	0	1	-2
AsO_4^{3-}	0	0	1	-3
$SH_3BO_4^-$	1	-1	1	-1
$SHMoO_4$	1	0	1	0
SH_2AsO_4	1	0	1	0
$SHAsO_4^-$	1	-1	1	-1
$SAsO_4^{2-}$	1	-2	1	-2

Note: A is an anion and x is the number of protons in the undissociated form of the acid.

3. APPLICATION OF THE CONSTANT CAPACITANCE MODEL TO SOILS

Application of the constant capacitance model to soil systems has been successful for describing phosphate [5], borate [6-11], selenite [12,13], arsenate [14,15], sulfate [16], and molybdate [17-19] adsorption.

3.1. Parameter estimation

3.1.1. Surface site density

The total number of reactive surface functional groups, SOH_T, is an important input parameter in the constant capacitance model. It has often been determined experimentally from potentiometric titration [16] or maximum adsorption data [5-7, 12-14, 17] and is related to the surface site density, N_s:

$$SOH_T = \frac{Sa10^{18}}{N_A} N_s \qquad (16)$$

where N_A is Avogadro's number and N_s has units of (sites nm^{-2}). Values of surface site density can be determined using a wide variety of methods. Results can vary by an order of magnitude between methods. The ability of the constant capacitance model to describe anion adsorption is sensitive to the value chosen for surface site density [20]. To allow the development of self-consistent parameter databases, Davis and Kent [21] recommended a surface site density value of 2.31 sites nm^{-2} for natural materials. This value has been used in the constant capacitance model to describe molybdate [18,19] and borate [8-11] adsorption on soils.

3.1.2. Capacitance

Capacitance values can be determined experimentally using linear extrapolations of titration data but exhibit great variability even for experiments using the same batch of a reference mineral [22]. For application of the constant capacitance model to soils, the capacitance value was either optimized to fit the ion adsorption data [12] or chosen from the literature. To describe borate [6-11], molybdate [17-19], and arsenate [14,15] adsorption, the capacitance was set at 1.06 F m^{-2}, considered optimum for aluminum oxide by Westall and Hohl [23]. For the development of self-consistent parameter databases and incorporation into speciation-transport models, a constant value of capacitance is necessary. The constant capacitance model was found to be insensitive to changes in capacitance value from 1.06 to 4.52 F m^{-2} for the iron oxide mineral, goethite [5].

3.1.3. Surface Complexation Constants

Protonation and dissociation constant values can be obtained from potentiometric titration data either by linear extrapolation or computer optimization [16], or obtained from the literature [5]. To describe molybdate [17-19] and arsenate [15] adsorption, the protonation constant, log K_+(int), was set to 7.35 and the dissociation constant, log K_-(int) was set to -8.95. These values were averages of a literature compilation of protonation-dissociation constants for aluminum and iron oxides [5].Ion surface complexation constants can be fit to the experimental data graphically, using the simplifying assumption that $\psi = 0$ [1]. Alternatively, ion surface complexation constants have generally been optimized using computer programs such as FITEQL [4].

Goodness of model fit is evaluated using the overall variance V in Y:

$$V_Y = \frac{SOS}{DF} \tag{17}$$

where SOS is the weighted sum of squares of the residuals and DF is the degrees of freedom. Use of the constant capacitance model to fit ion adsorption data by soils will be presented in detail in section 3.3.Recently, general prediction models have been developed to obtain ion surface complexation constants from easily measured soil chemical properties: cation exchange capacity, surface area, organic carbon content, inorganic carbon content, iron oxide content, and aluminum oxide content that correlate with soil adsorption capacity for trace element ions. This approach has been successfully applied to predict adsorption of borate [9-11], molybdate [19], and arsenate [15]. Use of the constant capacitance model to predict ion adsorption behavior by soils independently of experimental adsorption measurements using the general prediction models will be discussed in detail in section 3.5.

3.2. Experimental Methods

Trace element adsorption was investigated using 56 surface and subsurface samples from soils belonging to six different soil orders chosen to provide a wide range of soil chemical characteristics. Soil chemical characteristics are provided in Table 2. Soils Altamont to Yolo constitute a set of 23 soil series from the southwestern Unites States primarily California; soils Bernow to Teller constitute a set of 17 soil series from the midwestern United States, primarily Oklahoma.

3.2.1. Soil chemical characterization

Soil pH values were determined in 1:5 soil:water extracts [24]. Cation exchange capacities were measured by sodium saturation and magnesium extraction [25]. Ethylene glycol monoethyl ether adsorption was used to obtain surface areas [26]. Free iron and aluminum oxides were extracted [27]; Al and Fe concentrations were determined by inductively coupled plasma emission spectrometry. Carbon contents were obtained using a carbon coulometer. Organic C was calculated as the difference between total C measured after combustion at 950°C and inorganic C determined after acidification and heating.

3.2.2. Adsorption experiments

Adsorption experiments were carried out in batch systems to determine adsorption envelopes, amount of ion adsorbed as a function of solution pH at a fixed total ion concentration. Samples of soil (5 g for B and Mo and 1 g for As) were equilibrated with 25 mL of a 0.1 M NaCl background electrolyte solution on a shaker (20 h for B and Mo and 2 h for As). The equilibrating solution contained 0.463 mmol L^{-1} B, 0.292 mmol L^{-1} Mo or 0.02 mmol L^{-1} As(V) and had been adjusted to the desired pH range of 3 to 10 using 1 M HCl or 1 M NaOH. After reaction, the samples were centrifuged, decanted, analyzed for pH, filtered, and analyzed for B, Mo, or As concentration using inductively coupled plasma emission spectrometry. Additional experimental details are provided in Goldberg et al. [9] for B, Goldberg et al. [19] for Mo, and Goldberg et al. [15] for As(V) adsorption.

Adsorption isotherms, amount of ion adsorbed as a function of equilibrium solution ion concentration, were also determined for B adsorption. In this case, the equilibrating solutions contained 0, 0.0925, 0.185, 0.463, 0.925, 1.39, 2.31, 4.63, 9.25, 13.9, 18.5, or 23.1 mmol L^{-1} B. The average pH change for the highest B additions on all soils was 0.11 pH units.

Table 2
Chemical characteristics of soils

Soil series	Depth	pH	CEC	S	IOC	OC	Fe	Al
	cm		$mmol_c\,kg^{-1}$	$km^2\,kg^{-1}$	$g\,kg^{-1}$	$g\,kg^{-1}$	$g\,kg^{-1}$	$g\,kg^{-1}$
Altamont	0-25	5.90	152	0.103	0.0099	9.6	7.7	0.58
	25-51	5.65	160	0.114	0.011	6.7	8.2	0.64
	0-23	6.20	179	0.109	0.12	30.8	9.2	0.88
Arlington	0-25	8.17	107	0.0611	0.30	4.7	8.2	0.48
	25-51	7.80	190	0.103	0.16	2.8	10.1	0.60
Avon	0-15	6.91	183	0.0601	0.083	30.8	4.3	0.78
Bonsall	0-25	5.88	54	0.0157	0.13	4.9	9.3	0.45
	25-51	5.86	122	0.0329	0.07	2.1	16.8	0.91
Chino	0-15	10.2	304	0.159	6.4	6.2	4.7	1.64
Diablo	0-15	7.58	301	0.19	0.26	19.8	7.1	1.02
	0-15	7.42	234	0.13	2.2	28.3	5.8	0.84
Fallbrook	0-25	6.79	112	0.0683	0.023	3.5	6.9	0.36
	25-51	6.35	78	0.0285	0.24	3.1	4.9	0.21
Fiandcr	0-15	9.60	248	0.0925	6.9	4.0	9.2	1.06
Haines	20	9.05	80	0.0595	15.8	14.9	1.7	0.18
Hanford	0-10	8.40	111	0.0289	10.1	28.7	6.6	0.35
Hesperia	0-7.6	6.94	45	0.0309	0.018	4.9	3.2	0.34
Holtville	61-76	8.93	58	0.043	16.4	2.1	4.9	0.27
Imperial	Surface	8.11	222	0.196	18.6	9.1	6.1	0.38
	0-7.6	7.86	229	0.191	17.6	8.3	6.7	0.43
	15-46	8.58	198	0.106	17.9	4.5	7.0	0.53
Nohili	0-23	8.03	467	0.286	02.7	21.3	49.0	3.7
Pachappa	0-25	6.78	39	0.0151	0.026	3.8	7.6	0.67
	25-51	7.02	52	0.041	0.014	1.1	7.2	0.35
	0-20	8.98	122	0.0858	0.87	3.5	5.6	0.86
Porterville	0-7.6	6.83	203	0.137	0.039	9.4	10.7	0.90
Ramona	0-25	5.89	66	0.0279	0.02	4.4	4.5	0.42
	25-51	6.33	29	0.0388	0.018	2.2	5.9	0.40
Reagan	Surface	8.39	98	0.0588	18.3	10.1	4.6	0.45
Ryepatch	0-15	7.98	385	0.213	2.5	32.4	2.6	0.92
Scbree	0-13	5.99	27	0.0212	0.0063	2.2	6.0	0.46
Wasco	0-5.1	5.01	71	0.0309	0.009	4.7	2.4	0.42
Wyo		6.26	155	0.0539	0.014	19.9	9.5	0.89
Yolo	0-15	8.43	177	0.0730	0.23	11.5	15.6	1.13
Bernow	B	4.15	77.6	0.0464	0.0028	3.8	8.1	1.1
Canisteo	A	8.06	195	0.152	14.8	34.3	1.7	0.44
Dennis	A	5.27	85.5	0.0403	0.0014	18.6	12.9	1.7
	B	5.43	63.1	0.0724	0.0010	5.2	30.0	4.1
Dougherty	A	4.98	3.67	0.241	0.0010	7.0	1.7	0.28
Hanlon	A	7.41	142	0.0587	2.6	15.1	3.7	0.45
Kirkland	A	5.05	154	0.0421	0.014	12.3	5.6	0.80
Luton	A	6.92	317	0.169	0.099	21.1	9.1	0.99

Table 2
Chemical characteristics of soils

Soil Series	Depth	pH	CEC	S	IOC	OC	Fe	Al
	cm		$mmol_c\ kg^{-1}$	$km^2\ kg^{-1}$	$g\ kg^{-1}$	$g\ kg^{-1}$	$g\ kg^{-1}$	$g\ kg^{-1}$
Mansic	A	8.32	142	0.0422	16.7	10.1	2.7	0.40
	B	8.58	88.1	0.0355	63.4	9.0	1.1	0.23
Norge	A	3.86	62.1	0.0219	0.0010	11.6	6.1	0.75
Osage	A	6.84	377	0.134	0.59	29.2	15.9	1.4
	B	6.24	384	0.143	0.0100	18.9	16.5	1.3
Pond Creek	A	4.94	141	0.0354	0.0023	16.6	5.2	0.70
	B	6.78	106	0.0596	0.016	5.0	5.1	0.81
Pratt	A	5.94	23.9	0.0123	0.0026	4.2	1.2	0.18
	B	5.66	23.3	0.117	0.0007	2.1	0.92	0.13
Richfield	B	7.12	275	0.082	0.040	8.0	5.4	0.76
Summit	A	7.03	374	0.218	0.25	26.7	16.2	2.3
	B	6.23	384	0.169	0.0079	10.3	17.8	2.5
Taloka	A	4.88	47.4	0.087	0.0021	9.3	3.6	0.62
Teller	A	4.02	43.1	0.227	0.0008	6.8	3.2	0.53

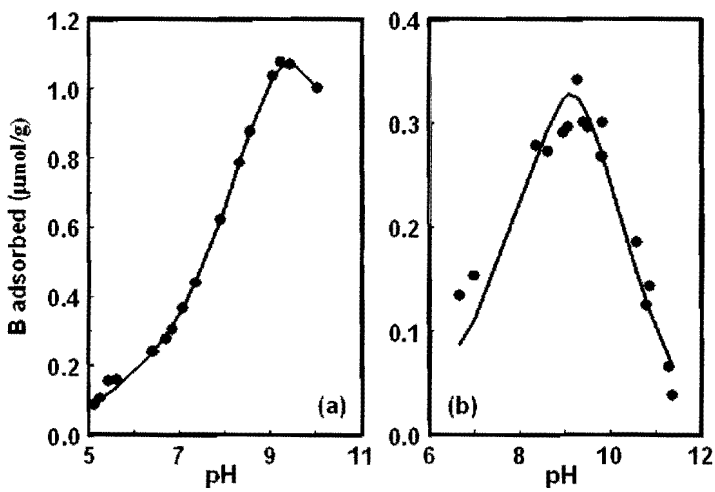

Fig. 2. Fit of the constant capacitance model to B adsorption: (a) Diablo clay; (b) Fallbrook loamy sand. Circles represent experimental data. Model fits are represented by solid lines. From Goldberg et al. [9].

3.3. Fitting ion adsorption data using the constant capacitance model

3.3.1. Borate

Borate adsorption as a function of solution pH was determined for 32 southwestern soil samples. Borate adsorption exhibited parabolic behavior, increasing with increasing solution pH, exhibiting an adsorption maximum around pH 9, and decreasing with further increases in solution pH (see Figs. 2 and 3b). Borate adsorption as a function of solution B concentration was determined for 23 southwestern soil samples. Borate adsorption increased with increasing solution B concentration tending toward a maximum at high solution B concentration (see Fig. 3a).

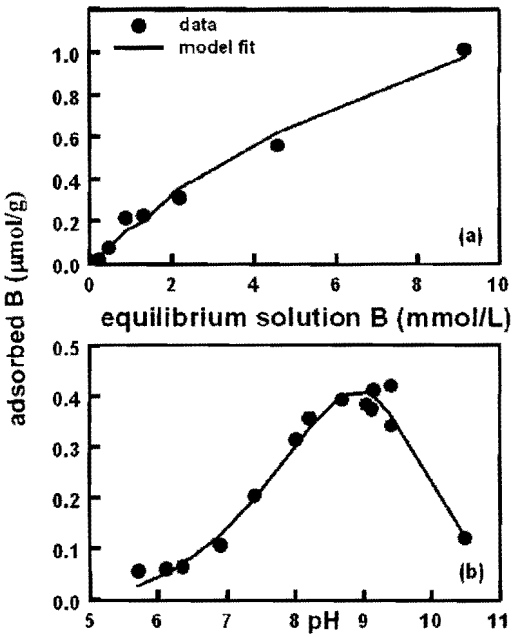

Fig. 3. Fit of the constant capacitance model to B adsorption on Bonsall soil: (a) isotherm; (b) envelope. Circles represent experimental data. Model fits are represented by solid lines.

The constant capacitance model was fit to the B adsorption envelopes by simultaneously optimizing the B surface complexation constant, log K_{B-}, the protonation constant, log K_{+}, and the dissociation constant, log K_{-} to improve model fit. The ability of the model to fit the experimental data is very good, as seen in Fig. 2. The constant capacitance model was also tested for its ability to describe B adsorption behavior as a function of both solution B concentration and solution pH simultaneously. As evidenced by Fig. 3, the model is able to quantitatively describe B adsorption as a function of both variables, simultaneously. Surface complexation constant values for the soils optimized with the constant capacitance model are presented in Table 3.

Table 3
Constant capacitance model surface complexation constants for B adsorption

Soil series	Depth (cm)	Using B adsorption envelopes Log K_{B}(int)	Log K_{+}(int)	Log K_{-}(int)
Altamont	0-25	-8.88	9.44	-10.90
Arlington	0-25	-8.58	8.73	-12.55
	25-51	-8.36	7.99	-12.01
Avon	0-15	-7.65	8.06	-11.08
Bonsall	25-51	-8.44	8.75	-11.96
Diablo	0-15	-8.33	8.12	-11.58
	0-15	-7.81	6.99	-10.52
Fallbrook	0-25	-8.62	8.82	-12.65
	25-51	-8.52	8.81	-11.85
Haines	20	-8.20	8.31	-11.82
Hanford	0-15	-7.38	7.70	-11.34
Holtville	61-76	-8.26	7.96	-11.75
Imperial	Surface	-8.24	7.66	-11.38
	0-7.6	-8.15	7.52	-11.17
	15-46	-7.95	7.88	-11.35
Ramona	25-51	-8.64	8.93	-12.10
Yolo	0-15	-7.90	7.39	-11.38
		Using B adsorption envelopes and isotherms		
Altamont	0-23	-6.53	5.32	-9.16
Arlington	0-25	-8.03	7.00	-11.07
Avon	0-15	-6.97	6.60	-10.06
Bonsall	0-25	-9.91	11.58	-14.12
Diablo	0-15	-7.77	6.40	-10.27
	0-15	-7.65	6.15	-10.24
Fallbrook	25-51	-7.91	8.36	-11.46
Fiander	0-15	-7.98	5.45	-9.57
Haines	20	-7.84	7.14	-11.10
Hanford	0-10	-7.14	7.06	-10.77
Hesperia	0-7.6	-8.24	8.38	-11.85
Holtville	61-76	-8.07	7.36	-11.41
Imperial	15-46	-7.74	6.71	-10.94
Nohili	0-23	-7.74	7.16	-9.96
Pachappa	0-25	-7.57	7.61	-10.90
	25-51	-8.48	8.26	-11.22
Porterville	0-7.6	-6.74	5.95	-9.09
Reagan	Surface	-7.36	6.71	-10.85
Ryepatch	0-15	-7.65	6.35	-10.12
Sebree	0-13	-6.57	6.21	-8.71
Wasco	0-5.1	-7.10	7.13	-9.70
Wyo		-10.05	11.91	-12.90
Yolo	0-15	-7.78	6.78	-11.15

Adapted from Goldberg et al. [9] and Goldberg [8].

3.3.2. Molybdate

Molybdate adsorption as a function of solution pH was determined for the 32 southwestern soil samples previously investigated for B adsorption. Molybdate adsorption exhibited a maximum in the pH range 2 to 5, decreased rapidly with increasing pH from pH 5 to 8, and was minimal above pH 9 (see Fig. 4).

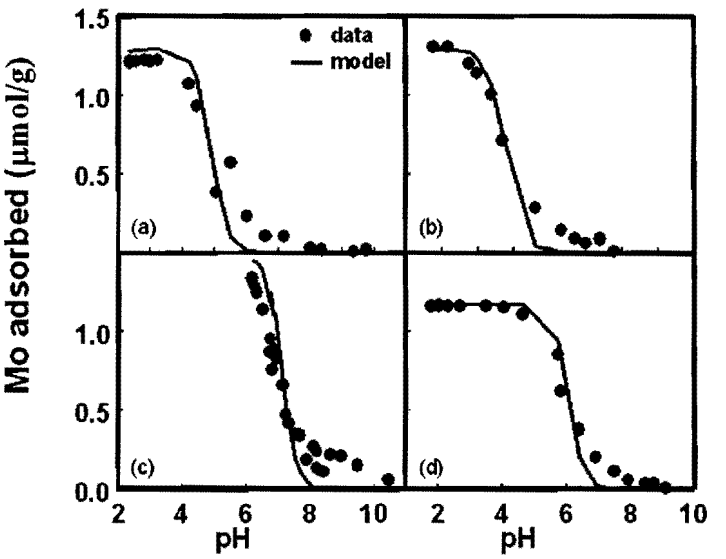

Fig. 4. Fit of the constant capacitance model to Mo adsorption: (a) Fallbrook loamy sand; (b) Hesperia sandy loam; (c) Nohili silt loam; (d) Wyo silt loam. Circles represent experimental data. Model fits are represented by solid lines. Adapted from Goldberg et al. [19].

The constant capacitance model provided a satisfactory fit to the Mo adsorption envelopes by only optimizing the monodentate Mo surface complexation constant, log K_{Mo}. Therefore, the protonation and dissociation constants were not optimized but fixed at log K_1 = 7.35 and log K_2 = -8.95, respectively. The ability of the model to fit Mo adsorption is shown in Fig. 4 for four soils. The model is well able to describe the Mo adsorption data at low pH, but deviates above pH values of 6 to 7. Table 4 provides values of the optimized monodentate Mo surface complexation constants for all the soils studied.

3.3.3. Arsenate

Arsenate adsorption as a function of solution pH was determined for 27 southwestern and 22 midwestern soil samples. Arsenate adsorption increased with increasing solution pH, exhibited a maximum in the pH range 6 to 7, and decreased with further increases in solution pH, as seen in Fig. 5.

Table 4
Constant capacitance model surface complexation constants for Mo adsorption

Soil Series	Depth (cm)	Log K_{Mo}(int)
Altamont	0-25	4.12
	25-51	3.45
	0-23	5.28
Arlington	0-25	4.76
Avon	0-15	5.89
Bonsall	0-25	4.85
Chino	0-20	5.03
Diablo	0-15	4.50
	0-15	4.32
Fallbrook	25-51	3.62
Fiander	0-15	5.26
Haines	20	5.69
Hanford	0-15	5.97
Hesperia	0-7.6	3.30
Holtville	61-76	5.44
Imperial	Surface	5.70
	0-7.6	5.20
	15-46	5.59
Nohili	0-23	6.87
Pachappa	0-15	5.18
	0-25	4.95
	0-25	4.56
	25-51	4.61
Porterville	0-7.6	4.78
	0-7.6	5.39
Ramona	0-25	3.58
Reagan	Surface	6.01
Ryepatch	0-15	5.15
Sebree	0-13	4.30
Wasco	0-5.1	3.17
Wyo		3.17
Yolo	0-15	5.26

Adapted from Goldberg et al. [19].

The constant capacitance model was fit to the As(V) adsorption envelopes by optimizing the three monodentate As(V) surface complexation constants, log K^1_{As}, log K^2_{As}, and log K^3_{As} simultaneously.

As was done previously for Mo adsorption, the protonation constant was fixed at log $K_+ = 7.35$ and the dissociation constant was fixed at log $K_- = -8.95$. The ability of the model to describe the As(V) adsorption data was very good for both surface and subsurface horizons (see Fig. 5). Values of the optimized monodentate As(V) surface complexation constants for the soils are listed in Table 5.

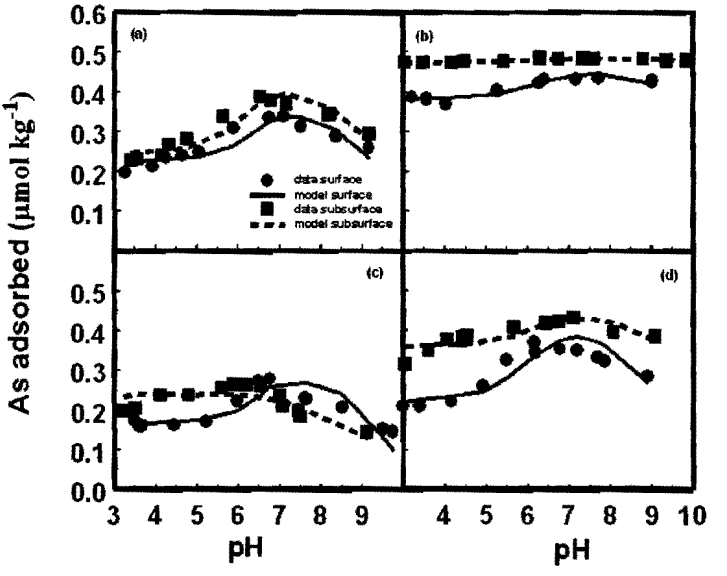

Fig. 5. Fit of the constant capacitance model to As(V) adsorption on southwestern soils (a, b) and Midwestern soils (c, d): (a) Altamont soil; (b) Pachappa soil; (c) Dennis soil; (d) Pond Creek soil. Circles and squares represent experimental data. Model fits are represented by solid and dashed lines. Adapted from Goldberg et al. [15].

3.4. General regression prediction models

A general regression modeling approach was used to relate the constant capacitance model surface complexation constants to the following soil chemical properties: cation exchange capacity, surface area, inorganic carbon content, organic carbon content, iron oxide content, and aluminum oxide content. An exploratory data analysis revealed that the surface complexation constants were linearly related to each of the log transformed chemical properties.Therefore the following initial regression model was specified for each of the surface complexation constants:

$$LogK_j = \beta_{0j} + \beta_{1j}(\ln CEC) + \beta_{2j}(\ln S) + \beta_{3j}(\ln IOC) + \beta_{4j}(\ln OC) + \beta_{5j}(\ln Fe) + \beta_{6j}(\ln Al) + \varepsilon \quad (18)$$

where the β_{ij} represent empirical regression coefficients and ε represents the residual error component.

Table 5
Constant capacitance model surface complexation constants for As(V) adsorption

Soil Series	Depth (cm)	Log K^1_{As}(int)	Log K^2_{As}(int)	Log K^3_{As}(int)
Altamont	0-25	9.99	3.92	-3.89
	25-51	10.09	4.41	-3.69
Arlington	0-25	9.57	2.04	-4.59
	25-51	9.95	2.92	-4.24
Avon	0-15	9.29	3.02	-4.52
Bonsall	0-25	9.50	2.77	-4.64
	25-51	10.90	3.64	-3.27
Diablo	0-15	9.26	3.14	-4.45
Fallbrook	0-25	10.02	3.00	-4.20
	25-51	9.56	2.84	-4.62
Fiander	0-15	10.08	2.10	-4.76
Haines	20	9.43	2.39	-4.01
Hanford	0-10	9.83	3.04	-4.16
Holtville	61-76	10.32	3.66	-3.88
Imperial	15-46	10.23	3.77	-3.77
Pachappa	0-25	9.67	3.55	-4.15
	25-51	10.03	3.06	-4.44
Porterville	0-7.6	10.36	3.89	-3.60
Ramona	0-25	9.58	2.79	-4.37
	25-51	9.96	2.99	-4.46
Reagan	Surface	9.66	2.94	-4.07
Ryepatch	0-15	9.40	3.07	-4.70
Sebree	0-13	9.64	3.28	-4.70
Wasco	0-5.1	9.65	3.31	-4.45
Wyo		10.36	3.67	-3.80
Yolo	0-15	10.00	3.96	-3.86
Dennis	A	10.99	5.02	-2.57
	B	12.51	6.93	-0.73
Dougherty	A	9.49	3.23	-4.21
Hanlon	A	10.11	3.18	-4.17
Kirkland	A	10.44	5.25	-3.14
Luton	A	10.46	4.46	-3.31
Mansic	A	9.71	3.05	-4.24
	B	10.21	2.58	-3.65
Norge	A	10.31	3.90	-3.99
Osage	A	11.75	5.08	-2.63
	B	12.26	5.97	-1.86
Pond Creek	A	10.02	4.44	-3.86
	B	10.85	4.98	-3.01
Pratt	A	9.14	2.56	-4.78
	B	9.26	2.55	-4.64
Richfield	B	10.00	3.85	-4.17
Taloka	A	10.25	4.11	-3.89
Teller	A	10.20	3.61	-4.34

Adapted from Goldberg et al. [15].

3.4.1. Borate

Results from the 17 soils for which simultaneous optimization of the protonation-dissociation constants and B surface complexation constant was possible were used to obtain the general regression prediction model for B adsorption. For borate, neither cation exchange capacity nor iron oxide content were found to be statistically significant after fitting Eq. (18) to each of the set of surface complexation constants. The surface area parameter was not found to be significantly related to either the protonation or the dissociation constant, after accounting for the remaining variables. Thus the prediction equations for obtaining surface complexation constants to describe B adsorption with the constant capacitance model are:

$$LogK_{B-} = -9.14 - 0.375\ln(S) + 0.167\ln(OC) + 0.111\ln(IOC) + 0.466\ln(Al) \quad (19)$$

$$LogK_{+} = 7.85 - 0.102\ln(OC) - 0.198\ln(IOC) - 0.622\ln(Al) \quad (20)$$

$$LogK_{-} = -11.97 + 0.302\ln(OC) + 0.0584\ln(IOC) + 0.302\ln(Al) \quad (21)$$

Additional details on the statistical analysis are provided in Goldberg et al. [9] and Goldberg [8]. Surface complexation constants obtained with the prediction equations are listed in Table 6 for B adsorption.

3.4.2. Molybdate

Results from 32 soils were used to obtain the general regression prediction model for Mo adsorption. For molybdate, neither the surface area nor the aluminum oxide content were found to be statistically significant after fitting Eq. (18) to the surface complexation constants. Thus the prediction equation for obtaining the monodentate Mo surface complexation constant to describe Mo adsorption with the constant capacitance model is:

$$LogK_{Mo} = 7.807 - 0.363\ln(CEC) + 0.219\ln(IOC) + 0.385\ln(OC) + 0.716\ln(Fe) \quad (22)$$

A "jack-knifing" procedure was preformed on this equation to assess its predictive ability. Jack-knifing represents a technique where each observation is sequentially set aside, the equation is reestimated without this observation, and the observation is then predicted from the remaining data using the reestimated equation. Monodentate Mo surface complexation constants obtained with the prediction equation and the jack-knifing procedure are provided in Table 7. Excellent agreement was obtained between the ordinary predictions and the jack-knifed estimates, indicating good predictive capability. Additional statistical details can be found in Goldberg et al. [19].

3.4.3. Arsenate

For arsenate, an initial analysis of the regression model presented by Eq. (18) yielded rather poor results. Additional statistical analyses revealed that the two groups of soils (18 midwestern soils and 26 southwestern soils) represented two distinct populations exhibiting different soil property/surface complexation constant relationships. A multivariate analysis of covariance established a common intercept and common ln(CEC) term for the general regression prediction equations for As(V) adsorption. The prediction equations for obtaining monodentate As(V) surface complexation constants to describe As(V) adsorption with the constant capacitance model are:

Table 6
Constant capacitance model surface complexation constants predicted for B adsorption

Soil series	Depth (cm)	Log K_{B1}(int)	Log K_{+}(int)	Log K_{-}(int)
Southwestern				
Altamont	0-25	-8.71	8.83	-11.79
	0-23	-8.03	8.00	-11.10
Bonsall	0-25	-8.19	8.59	-11.85
Fiander	0-15	-7.77	7.29	-11.42
Hesperia	0-7.6	-8.52	9.16	-12.05
Nohili	0-23	-7.43	6.53	-10.59
Pachappa	0-25	-8.26	8.69	-11.90
	25-51	-8.89	9.34	-12.50
Porterville	0-7.6	-8.51	8.33	-11.51
Ramona	0-25	-8.38	9.01	-12.01
Reagan	Surface	-7.73	7.54	-11.34
Ryepatch	0-15	-7.91	7.37	-10.89
Sebree	0-13	-8.48	9.26	-12.26
Wasco	0-5.1	-8.72	9.17	-12.04
Wyo		-8.21	8.47	-11.35
Midwestern				
Bernow	B	-8.35	8.79	-11.87
Canisteo	A	-7.92	7.47	-10.99
Dennis	A	-7.93	8.53	-11.31
	B	-7.98	8.17	-11.44
Dougherty	A	-9.64	9.82	-12.17
Hanlon	A	-7.89	7.88	-11.33
Kirkland	A	-8.11	8.58	-11.53
Luton	A	-8.22	8.01	-11.19
Mansic	A	-7.68	7.63	-11.38
	B	-7.74	7.73	-11.51
Norge	A	-8.20	9.15	-11.72
Osage	A	-7.70	7.38	-10.87
	B	-8.29	8.28	-11.26
Pond Creek	A	-8.26	8.99	-11.58
	B	-8.36	8.63	-11.79
Pratt	A	-8.72	9.96	-12.41
	B	-9.97	10.49	-12.79
Richfield	B	-8.33	8.44	-11.61
Summit	A	-7.78	7.27	-10.80
	B	-8.20	8.01	-11.27
Taloka	A	-8.75	9.14	-11.80
Teller	A	-9.35	9.46	-12.00

Adapted from Goldberg et al. [9] and Goldberg et al. [10].

Table 7
Constant capacitance model surface complexation constants predicted for Mo adsorption

Soil Series	Depth (cm)	Predicted Log K_{Mo}(int)	Jack-knife predicted Log K_{Mo}(int)
Altamont	0-25	4.27	4.28
	25-51	4.18	4.28
	0-23	5.33	5.34
Arlington	0-25	4.91	4.92
Avon	0-15	4.70	4.46
Bonsall	0-25	5.08	5.12
Chino	0-20	4.90	4.87
Diablo	0-15	4.95	5.01
	0-15	5.51	5.65
Fallbrook	25-51	4.45	4.51
Fiander	0-15	5.31	5.32
Haines	20	5.20	4.99
Hanford	0-15	6.21	6.30
Hesperia	0-7.6	3.95	4.05
Holtville	61-76	5.33	5.30
Imperial	Surface	5.59	5.58
	0-7.6	5.60	5.65
	15-46	5.45	5.43
Nohili	0-23	6.72	6.59
Pachappa	0-15	4.71	4.67
	0-25	4.55	4.61
	0-25	4.61	4.61
	25-51	3.85	3.65
Porterville	0-7.6	4.68	4.67
	0-7.6	4.68	4.61
Ramona	0-25	4.04	4.08
Reagan	Surface	5.72	5.67
Ryepatch	0-15	4.83	4.71
Sebree	0-13	4.05	3.99
Wasco	0-5.1	3.41	3.48
Wyo		4.76	4.68
Yolo	0-15	5.47	5.50
Norge	0-15	3.99	
Pond Creek	0-15	3.90	
Taloka	0-15	3.79	
Tellcr	0-15	3.42	

Adapted from Goldberg et al. [19].

$$LogK^{1}_{As} = 10.639 - 0.107\ln(CEC) + 0.078\ln(IOC) - 0.365\ln(OC) + 1.087\ln(Fe) + 0.094\ln(S) \quad (23)$$

$$LogK^{2}_{As} = 3.385 - 0.083\ln(CEC) - 0.002\ln(IOC) - 0.400\ln(OC) + 1.360\ln(Fe) + 0.018\ln(S) \quad (24)$$

$$LogK^{3}_{As} = -2.579 - 0.296\ln(CEC) + 0.115\ln(IOC) - 0.570\ln(OC) + 1.382\ln(Fe) - 0.004\ln(S) \quad (25)$$

for midwestern soils and:

$$LogK^{1}_{As} = 10.639 - 0.107\ln(CEC) + 0.022\ln(IOC) - 0.143\ln(OC) + 0.385\ln(Fe) + 0.256\ln(S) \quad (26)$$

$$LogK^{2}_{As} = 3.385 - 0.083\ln(CEC) - 0.061\ln(IOC) - 0.104\ln(OC) + 0.313\ln(Fe) + 0.247\ln(S) \quad (27)$$

$$LogK^{3}_{As} = -2.579 - 0.296\ln(CEC) + 0.024\ln(IOC) - 0.085\ln(OC) + 0.363\ln(Fe) - 0.376\ln(S) \quad (28)$$

for southwestern soils.

Monodentate As(V) surface complexation constants obtained with the prediction equations and the jack-knifing procedure are listed in Table 8. The jack-knifing procedure indicated good general agreement between ordinary predictions and jack-knife estimates suggesting predictive capability. Additional statistical analyses are provided in Goldberg et al. [15].

Table 8
Constant capacitance model surface complexation constants predicted for As(V) adsorption

Soil Series	Depth (cm)	Predicted $LogK^{1}_{As}$	Predicted $LogK^{2}_{As}$	Predicted $LogK^{3}_{As}$	Jack-knife $LogK^{1}_{As}$	Jack-knife $LogK^{2}_{As}$	Jack-knife $LogK^{3}_{As}$
Southwestern							
Altamont	0-25	9.88	3.56	-4.10	9.86	3.51	-4.13
	25-51	9.98	3.56	-4.08	9.96	3.45	-4.13
Arlington	0-25	9.99	3.20	-4.15	10.01	3.27	-4.12
	25-51	10.20	3.33	-4.10	10.24	3.40	-4.08
Avon	0-15	9.38	3.22	-4.42	9.40	3.28	-4.39
Bonsall	0-25	9.92	3.20	-4.15	9.98	3.25	-4.09
	25-51	10.47	3.56	-3.82	10.35	3.53	-3.98
Diablo	0-15	9.90	3.51	-3.96	10.03	3.58	-3.86
Fallbrook	0-25	9.93	3.30	-4.27	9.92	3.32	-4.27
	25-51	9.68	2.85	-4.57	9.70	2.85	-4.56
Fiander	0-15	10.14	3.06	-4.14	10.15	3.30	-3.98
Haines	20	9.33	2.60	-4.45	9.28	2.69	-4.64

Table 8
Constant capacitance model surface complexation constants predicted for As(V) adsorption

Soil Series	Depth (cm)	Predicted $LogK^1_{As}$	Predicted $LogK^2_{As}$	Predicted $LogK^3_{As}$	Jack-knife $LogK^1_{As}$	Jack-knife $LogK^2_{As}$	Jack-knife $LogK^3_{As}$
Hanford	0-10	9.53	2.92	-4.28	9.38	2.86	-4.34
Holtville	61-76	9.97	2.67	-4.26	9.85	2.35	-4.38
Imperial	15-46	10.10	2.98	-4.08	10.06	2.78	-4.16
Nohili	0-23	10.74	4.04	-3.17			
Pachappa	0-25	9.91	3.26	-4.15	9.94	3.22	-4.15
	25-51	10.05	3.16	-4.33	10.05	3.18	-4.30
Porterville	0-7.6	10.14	3.68	-3.84	10.10	3.64	-3.89
Ramona	0-25	9.55	3.02	-4.59	9.55	3.06	-4.63
	25-51	9.93	3.19	-4.18	9.92	3.22	-4.14
Reagan	Surface	9.74	2.84	-4.18	9.76	2.83	-4.20
Ryepatch	0-15	9.50	3.11	-4.26	9.54	3.13	-4.06
Sebree	0-13	9.76	3.11	-4.41	9.80	3.07	-4.33
Wasco	0-5.1	9.46	3.04	-4.59	9.39	2.95	-4.64
Wyo		9.79	3.62	-4.06	9.66	3.60	-4.12
Yolo	0-15	10.09	3.51	-3.93	10.11	3.42	-3.94
Midwestern							
Bernow	B	11.21	5.29	-2.40			
Canisteo	A	9.39	2.21	-5.11			
Dennis	A	11.06	5.28	-2.77	11.08	5.34	-2.82
	B	12.50	6.97	-0.83	12.48	7.12	-1.16
Dougherty	A	9.69	3.21	-4.13	10.14	3.16	-3.95
Hanlon	A	10.35	3.61	-3.66	10.40	3.71	-3.55
Kirkland	A	10.42	4.26	-3.60	10.42	4.14	-3.65
Luton	A	10.96	4.66	-3.23	11.10	4.72	-3.20
Mansic	A	10.26	3.34	-3.65	10.50	3.45	-3.41
	B	9.47	2.19	-4.53	8.86	1.88	-5.26
Norge	A	10.37	4.46	-3.47	10.38	4.61	-3.34
Osage	A	11.55	5.27	-2.49	11.47	5.34	-2.43
	B	11.43	5.50	-2.66	11.19	5.36	-2.90
Pond	A	10.09	4.04	-4.05	10.11	3.91	-4.11
Creek	B	10.73	4.53	-3.09	10.71	4.44	-3.10
Pratt	A	9.09	2.73	-4.75	9.06	2.85	-4.72
	B	9.17	2.69	-4.87	9.12	2.77	-5.01
Richfield	B	10.62	4.34	-3.45	10.73	4.42	-3.33
Summit	A	11.58	5.34	-2.51			
	B	11.73	5.85	-2.24			
Taloka	A	10.09	3.88	-3.92	10.07	3.85	-3.92
Teller	A	10.10	3.87	-3.99	10.08	3.95	-3.89

Adapted from Goldberg et al. [15].

3.5. Predicting ion adsorption behavior using the constant capacitance model

3.5.1. Borate

The prediction equations, Eqs. (19)-(21), were used to predict surface complexation constants for 15 soils that had not been used to obtain the general regression model. The constant capacitance model was then used to predict B adsorption on these soils using the predicted surface complexation constants. Since the data from these 15 soils had not been used to develop the prediction equations, this is a completely independent evaluation of the model's ability to predict B adsorption. This is in contrast to regression models that fit soil adsorption data. The distinction is that by combining Eqs. (19)-(21) and the constant capacitance model, only soil chemical properties and not adsorption data are used to predict B adsorption behavior on a specific soil.

The ability of this approach to predict B adsorption on the 15 soils is indicated in Fig. 6. The model always predicted the shape of the adsorption envelope and the pH of maximum B adsorption. Prediction was very reasonable for most soils. Prediction of B adsorption for the Nohili soil (Fig. 6l) was quantitative, despite the fact that several of the chemical characteristics (CEC, S, Fe, Al) of this soil fell outside the range for the 17 soils used to obtain the prediction equations. This result suggests that the prediction equations may have predictive capability for other soils outside the present ranges of soil chemical characteristics.

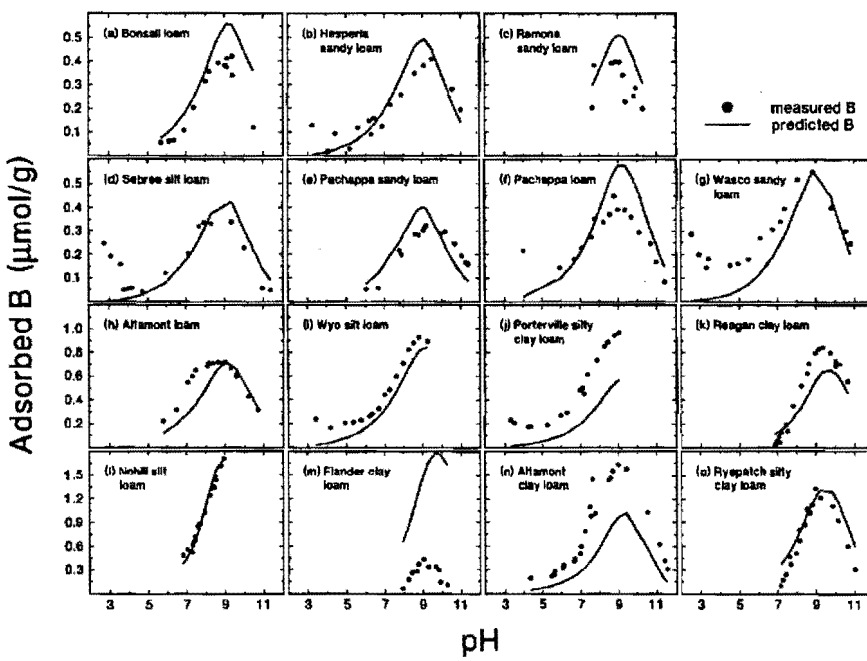

Fig. 6. Constant capacitance model prediction of B adsorption by soils not used to obtain the prediction equations. Circles represent experimental data. Model predictions are represented by solid lines. From Goldberg et al. [9].

The prediction equations, developed from describing B adsorption envelopes by a set of soils from the southwestern U.S., were used to predict B adsorption isotherms of a set of midwestern soils. For the majority of the soils, the predictions were able to accurately describe B adsorption. The model predictions were obtained independent of any experimental measurement of B adsorption on these soils using only values of soil chemical parameters. The constant capacitance model was well able to predict B adsorption on midwestern soils as presented in Fig. 7.

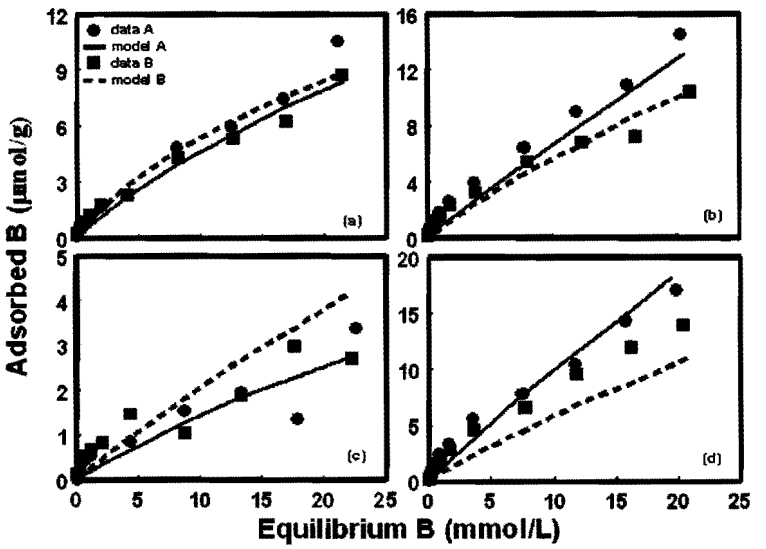

Fig. 7. Constant capacitance model prediction of B adsorption isotherms for Midwestern soils not used to obtain the prediction equations: (a) Mansic soil; (b) Osage soil; (c) Pond Creek soil; (d) Summit soil. Experimental data are represented by circles (A horizon) and squares (B horizon). Model predictions are represented by solid lines (A horizon) and dashed lines (B horizon). Adapted from Goldberg et al. [10].

Boron adsorption on 15 soils samples constituting five depths of each of three sites in one quarter section of a field in the San Joaquin Valley of California, USA was investigated as a function of solution pH. The constant capacitance model was able to predict B adsorption using surface complexation constants calculated from the above prediction equations. The model was also able to predict B adsorption at all of the depths (0-30, 30-60, 60-90, 90-120, 120-150 cm) using the surface complexation constants predicted with the chemical properties of one of the surface depths and a surface area calculated from clay content using the equation [11]:

$$S = 5.654 + 348.9(clay\%) \tag{29}$$

These results indicate that, within a given field, reasonable estimates of surface complexation constants can be obtained from the measurement of soil chemical properties, regardless of depth or position within the field. This finding significantly reduces the need for tedious, time-consuming laboratory experiments of B adsorption. These predictions are suitable for transport modeling applications.

3.5.2. Molybdate

The prediction equation, Eq. (22), was used to predict monodentate Mo surface complexation constants for 36 soils. The constant capacitance model was then used to predict Mo adsorption on the soils. Figure 8 depicts the ability of the model to predict Mo adsorption. Prediction was at least semi-quantitative for all soils. For the Nohili and Wyo soils, the model predicted results were almost as close to the experimental data as the fitted results (compare Fig. 8c with Fig. 4c and Fig. 8d with Fig. 4d). Model predictions for the Fallbrook (Fig. 8a) and Hesperia (Fig 8b) soils showed the greatest deviation from experimental adsorption data of any of the soils.

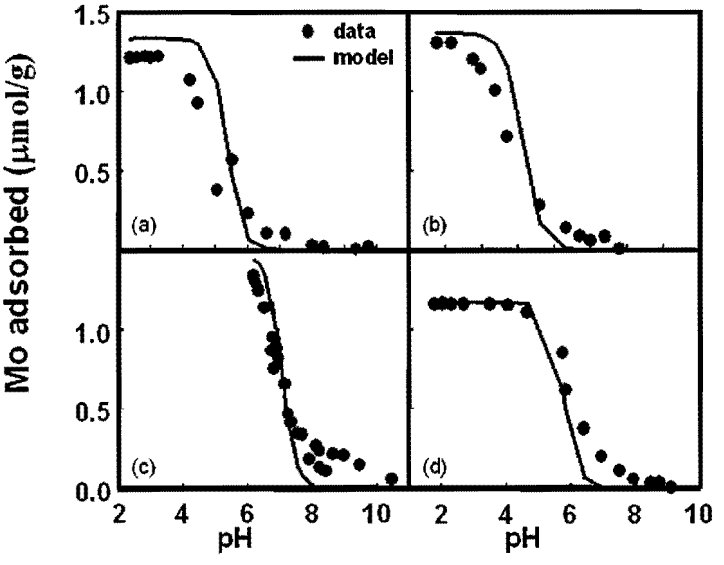

Fig. 8. Constant capacitance model prediction of Mo adsorption by soils: (a) Fallbrook loamy sand; (b) Hesperia sandy loam; (c) Nohili silt loam; (d) Wyo silt loam. Circles represent experimental data. Model predictions are represented by solid lines. Adapted from Goldberg et al. [19].

3.5.3. Arsenate

The monodentate As(V) surface complexation constants were predicted using the prediction equations, Eqs. (23)-(25), for 22 midwestern soils and using the prediction equations, Eqs.

(26)-(28), for 27 southwestern soils. The constant capacitance model was then used to predict As(V) adsorption on the soils. The ability of the model to predict As(V) adsorption is shown in Fig. 9 for five soils not used to obtain the prediction equations. Prediction of As(V) adsorption by the Bernow soil (Fig. 9a) and the two Summit (Fig. 9c) soil horizons was good. Prediction of As(V) adsorption by the Nohili soil (Fig. 9d) deviated from the experimental adsorption data by 30% or less, a reasonable result considering that the prediction was obtained without optimization of any adjustable parameters. Prediction of As(V) adsorption by the Canisteo soil was very poor (Fig. 9b).

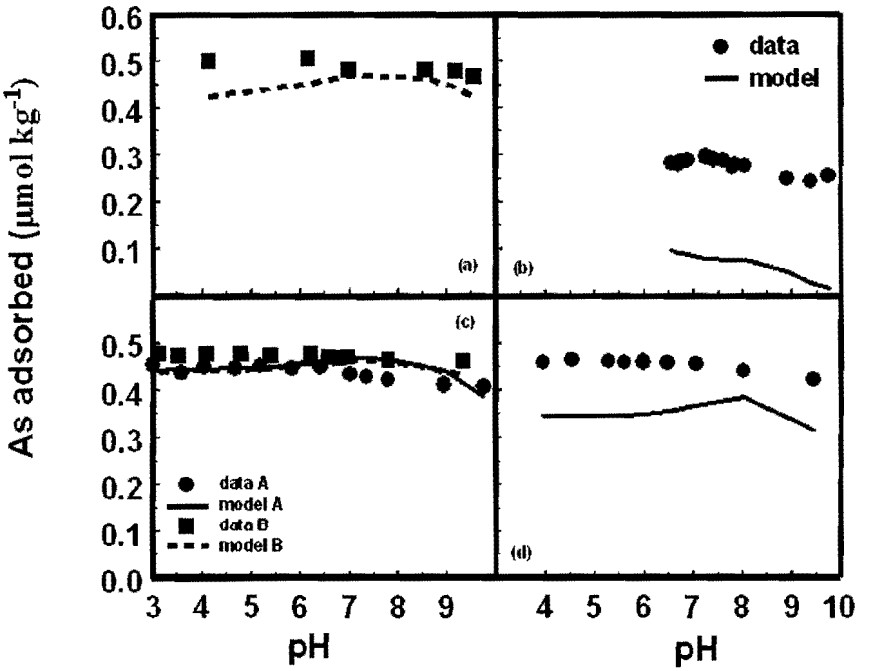

Fig. 9. Constant capacitance model prediction of As(V) adsorption by soils not used to obtain the prediction equations: (a) Bernow soil; (b) Canisteo soil; (c) Summit soil; (d) Nohili soil. Experimental data are represented by circles (A horizon) and squares (B horizon). Model predictions are represented by solid lines (A horizon) and dashed lines (B horizon). From Goldberg et al. [15].

3.6. Analysis of optimal management of high B waters used for irrigation

Water quality criteria consider waters above 1 mg B L^{-1} to be potentially toxic to B sensitive plant species [28]. Only a few agronomic crops can tolerate concentrations in excess of 10 mg B L^{-1}. Thus toxic concentrations of B in drainage water are often one of the major limitations to drainage water reuse in the western USA. As mentioned earlier, there is a need to develop management practices for use of these waters. The examples provided below [29], demonstrate the predictive capability of the constant capacitance model for B adsorption and its utility as a management tool when combined with water and solute transport in the

UNSATCHEM speciation-transport model [30].

The use of the UNSATCHEM model for irrigation management of high B waters is demonstrated by the following example [29]. Irrigation drainage water from the westside of the Central Valley of California typically contains 0.4 to 0.8 mmol B L^{-1} and has an electrical conductivity of 8-14 dS m^{-1}. This geographic area is adversely affected by high surface salinity due in major part to high water tables caused by restrictions on discharge of drainage water. Use of the drainage water for irrigation would drop the water table and decrease the soil salinity. However, these waters are typically considered to be unusable for irrigation, or usable only on salt and B tolerant crops. Using the traditional steady state approach (in this case no B adsorption-desorption), the solution B concentration would increase in the soil proportionately to the chloride concentration. Thus, the recommendation when irrigating with high B water, is to increase leaching to maintain a lower B concentration in the root zone. In the present simulations, we selected a B concentration of 0.8 mmol L^{-1}. We assumed that either a limited quantity of high quality water was available or that there was some rainfall, but that the high quality water needed to be supplemented with low quality water. Although low quality water is often not usable for sustained agricultural production, it can be utilized either in a cyclic fashion with higher quality water where the soil is periodically reclaimed via leaching, or the waters can be used on separate fields on crops of varying B tolerance.

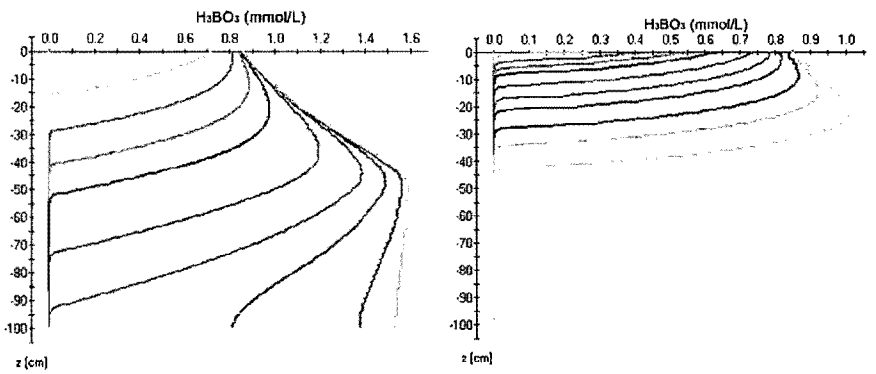

Fig. 10. Change in boron concentration with depth and time (0, 10, 20, 30, 40, 50, 60, 70, 80, 90 and 100 days) for a leaching fraction of 0.5 and soil surface area: a) 100 m^2 g^{-1}; b) 1000 m^2 g^{-1} [29].

A uniform root distribution and uniform water uptake in a 50 cm root zone was considered in a soil profile initially free of B. Model parameter values for B adsorption were constant with depth. In the simulation shown in Figure 10a [29], evapotranspiration was input as 1 cm day^{-1} with irrigation applications corresponding to an average input of 2 cm day^{-1}. This corresponds to a leaching fraction of 0.5 (where leaching fraction is defined as the fraction of water applied that is not used by evapotranspiration and is drained from the root zone). A total of 200 cm of water was applied during the 100 day growing season. The surface area of the soil was taken as 100 m^2 g^{-1}, corresponding to a soil with relatively low B absorption capacity. The high leaching combined with the low B absorption capacity of this

sandy soil causes a rapid advance of the B front into the soil, as shown in Figure 10a. Each line corresponds to a time increment of 10 days. The B concentration is initially uniform at 0 mmol L^{-1} at day 0. A quasi-steady state profile is established in the root zone after 80 days, with a maximum soil B concentration of 1.6 mmol L^{-1}.

Figure 10b shows a simulation similar to that depicted in Figure 10a except that the B adsorption capacity of the soil is now taken as 1000 m^2 g^{-1}, corresponding to a high clay content soil having a correspondingly high B absorption capacity [29]. The higher adsorption capacity (or surface site density) results in greater B adsorption, a steeper B front, and less rapid movement of B into the soil profile. This profile is still very far from steady state after 100 days of irrigation. Note that the solution B concentrations are significantly lower than those shown in Figure 10a.

The simulations shown in Figure 11 are similar to those presented in Figure 10 except that now the leaching fraction is 0.1. The daily evapotranspiration is still 1.0 cm day^{-1}, however, the water application is reduced to 1.11 cm day^{-1}. In these simulations, a total of 1.11 m of water was applied over the irrigation season. As shown in Figure 11a, after 100 days the profile is still not at steady state and the B front is just reaching the 100 cm depth. The maximum soil B concentration will eventually reach 8.0 mmol L^{-1}. The simulation shown in Figure 11b is for a leaching fraction of 0.1 and a soil with high surface area. After 100 days, the B concentration front extends only to 25 cm and the maximum B concentration is only 0.80 mmol L^{-1}, much lower than the steady state value of 8.0 mmol B L^{-1}, and just slightly greater than the B concentration of the irrigation water. Consistent with the high soil surface area and large number of adsorption sites, the B concentration front is relatively steep.

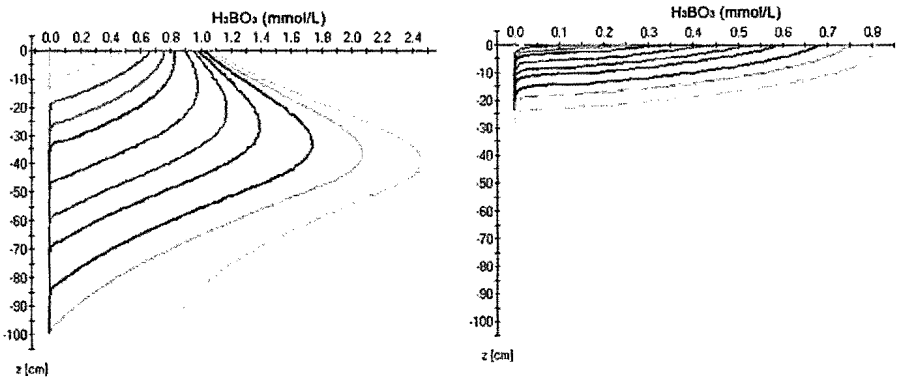

Fig. 11. Change in boron concentration with depth and time (0, 10, 20, 30, 40, 50, 60, 70, 80, 90 and 100 days) for a leaching fraction of 0.1 and soil surface area: a) 100 m^2 g^{-1}; b) 1000 m^2 g^{-1} [29].

The mean root zone B concentrations as a function of time are presented in Figure 12 for all four simulations [29]. The simulations indicate that, for a soil with high B adsorption capacity, there is little B hazard during the initial cropping season. The highly leached high surface area soil had a higher root zone B concentration throughout the growing season than did the other scenarios. At steady state, the lower leaching fraction management eventually resulted in considerably higher soil B concentrations than did the higher leaching fraction. However, the agricultural system can be managed in a continuous transitional state. Under

this scenario, the recommended practice (in the absence of salinity considerations) would be minimal water applications. This recommendation is counter to the conventional management recommendation that is based on the steady state analysis. The mean B concentration in the root zone is sufficiently low that many crops could be grown without yield loss. Sustained management would require winter rains, leaching with higher quality water, or cyclic use of the high B irrigation water and a lower B water in alternate years.

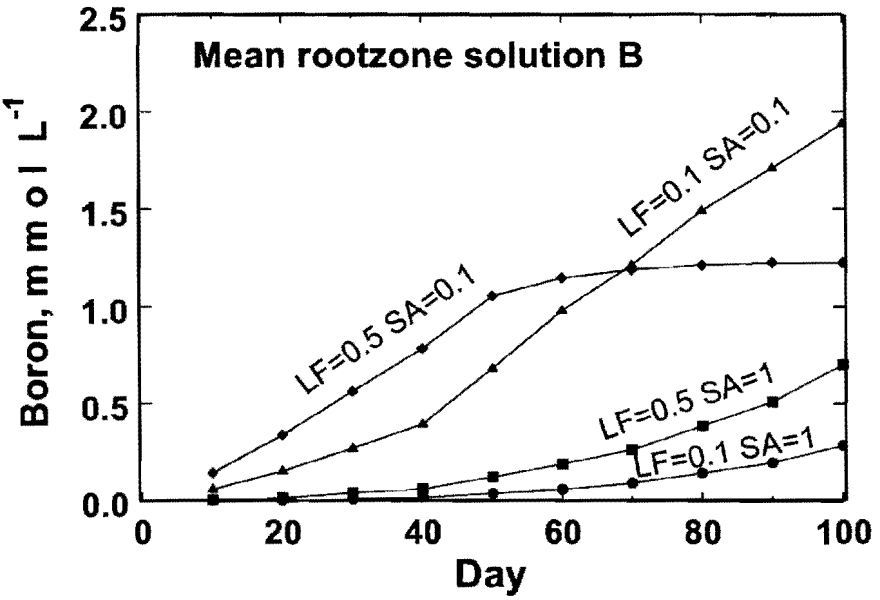

Fig. 12. Mean root zone soil solution B concentration with time as related to leaching fraction (LF) and soil surface area (SA), expressed in 10^3 x m^2 g^{-1} [29].

As shown in Figure 12, the low surface area soils rapidly increase in B concentration in the root zone, at both high and low leaching fractions. During the early portions of the season, the low leaching management results in lower root zone B concentrations, as steady state values are not yet achieved. At day 70, there is a crossover where the low leaching fraction management results in higher root zone B concentrations. In this scenario, it would appear preferable to utilize a low leaching approach, at least early in the irrigation season and especially if B sensitivity is greater during early stages of crop growth. For low surface area soils, most crops would have significant yield reduction due to B toxicity. At the point where the curves cross, at day 70, it would be beneficial to switch from low to high leaching fraction. Many vegetable crops with high B sensitivity also have a short growing season. In addition, B damage is not instantaneous, but rather cumulative, so that crops sensitive to 0.5 mmol B L^{-1} could likely be grown under this scenario during a 70-90 day growing season.

REFERENCES

[1] P.W. Schindler, B. Fürst, R. Dick and P.U. Wolf, J. Colloid Interface Sci., 55 (1976) 469.
[2] W. Stumm, R. Kummert and L. Sigg, Croatica Chem. Acta, 53 (1980) 291.
[3] G. Sposito, J. Colloid Interface Sci., 91 (1983) 329.
[4] A.L. Herbelin and J.C. Westall, FITEQL: A computer program for determination of chemical equilibrium constants from experimental data, Rep. 96-01, Version 3.2, Dep. of Chemistry, Oregon State Univ., Corvallis, 1996.
[5] S. Goldberg and G. Sposito, Soil Sci. Soc. Am. J., 48 (1984) 779.
[6] S. Goldberg and R.A. Glaubig, Soil Sci. Soc. Am. J., 50 (1986) 1173.
[7] S. Goldberg, Soil Sci. Soc. Am. J. 63 (1999) 823.
[8] S. Goldberg, Vadose Zone J., 3 (2004) 676.
[9] S. Goldberg, S.M. Lesch and D.L. Suarez, Soil Sci. Soc. Am. J., 64 (2000) 1356.
[10] S. Goldberg, D.L. Suarez, N.T. Basta and S.M. Lesch, Soil Sci. Soc. Am. J., 68 (2004) 795.
[11] S. Goldberg, D.L. Corwin, P.J. Shouse and D.L. Suarez, Soil Sci. Soc. Am. J., 69 (2005) 1379.
[12] G. Sposito, J.C.M. deWit and R.H. Neal, Soil Sci. Soc. Am. J., 52 (1988) 947.
[13] S. Goldberg and R.A. Glaubig, Soil Sci. Soc. Am. J., 52 (1988) 954.
[14] S. Goldberg and R.A. Glaubig, Soil Sci. Soc. Am. J., 52 (1988) 1297.
[15] S. Goldberg, S.M. Lesch, D.L. Suarez and N.T. Basta, Soil Sci. Soc. Am. J., 69 (2005) 1389.
[16] Z.S. Kooner, P.M. Jardine and S. Feldman, J. Environ. Qual., 24 (1995) 656.
[17] S. Goldberg, H.S. Forster and C.L. Godfrey, Soil Sci. Soc. Am. J., 60 (1996) 425.
[18] S. Goldberg, C. Su and H.S. Forster, *In* E.A. Jenne (ed.), Adsorption of metals by geomedia: Variables, mechanisms, and model applications, Proc. Am. Chem. Soc. Symp., Academic Press, San Diego (1998) 401.
[19] S. Goldberg, S.M. Lesch and D.L. Suarez, Soil Sci. Soc. Am. J., 66 (2002) 1836.
[20] S. Goldberg, J. Colloid Interface Sci., 145 (1991) 1.
[21] J.A. Davis and D.B. Kent, Rev. Mineral., 23 (1990) 177.
[22] S. Goldberg, Adv. Agron., 47 (1992) 233.
[23] J.C. Westall and H. Hohl, Adv. Colloid Interface Sci., 12 (1980) 265.
[24] G.W. Thomas, in D.L. Sparks et al. (eds.) Methods of soil analysis. Part 3—Chemical methods, Soil Science Society of America Book Series 5, Soil Science Society of America, Madison (1996) 475.
[25] J.D. Rhoades, in A.L. Page et al. (eds.) Methods of soil analysis, Part 2, 2nd ed. Agronomy Monograph 9, American Society of Agronomy, Madison (1982), 149.
[26] L.J. Cihacek and J.M. Bremner, Soil Sci. Soc. Am. J. 43 (1979) 821.
[27] D.E. Coffin, Can. J. Soil Sci., 43 (1963) 7.
[28] R.S. Ayers and Wescot, Water quality for agriculture. Foreign Agricultural Organization, Irrigation and Drainage Paper 29, Rev. 1, Foreign Agricultural Organization, Rome, 1985.
[29] D.L. Suarez, in Proc. Meeting of the International Union of Soil Scientist, August 14-21, 2002, Bangkok, Thailand, Symposium 34, (2002) 1096-1.
[30] D.L. Suarez and J. Simunek, Soil Sci. Soc. Am. J., 61 (1997) 1633.